scientific reports

OPEN

Experimental and theoretical validation for transmutation of palladium at electrochemical interfaces

Trilochan Gadly[1,10]✉, Suhas Phapale[2,10], Sunita Gamre[1], Pankaj Jain[3], Harishyam Kumar[4], Sanjeev Kumar Poudel[5], Shraddha Desai[5], Arup Kumar Pathak[2,10], Ashutosh Srivastava[6], Amit Kumar[7], Rupali Pal[8], Pallavi Chandwadkar[9], Celin Acharya[9,10], A. K. Bakshi[8,10], Salil Varma[2,10], Birija S. Patro[1,10] & Dibakar Goswami[1,10]✉

Electrolysis of D_2O may be used as a portable neutron source with numerous applications without the complexity of huge reactor operations. Herein, we report reproducible fast neutron generation by electrolysis of D_2O using palladium cathode and platinum anode, which was detected with diamond detector, gas filled ^{3}He detectors after thermalisation with high density polythene, as well as novel epoxy resin and CR-39 detectors. Notably, a highly reproducible neutron generation at electrochemical surfaces of palladium electrode was observed and signature transmutation via Pd (d, n) Ag was corroborated. This was further explained using a theoretical model based on second order quantum perturbation theory.

The need of a neutron source in many strategic and non-strategic applications, including security, environmental and geological applications, medical oncology, biophysics, and in particular, boron neutron capture therapy (BNCT), is tremendous[1]. However, neutron sources are not easily accessible as they are expensive and require complex operating procedures. Hence, fabrication of portable and reproducible neutron source is of utmost importance. Ever since Fleishmann and Pons reported their cold fusion experiment in 1989 on neutron generation via electrolysis of water using Pd cathode[2], it was considered as an ideal neutron source for on-site applications. Many researchers worldwide had tried to reproduce and advance the experiment[3]. However, most of the studies were unsuccessful and unexplained due to lack of a proper theory explaining the phenomenon. Additionally, unsolved problems viz. sporadic radiation, radiation levels just above the background have been a major cause of general acceptability of cold fusion reaction as a neutron source. The offered hypotheses and theory behind the proposed mechanism are also contested due to the lack of exceptionally high temperatures or a massive quantity of electromagnetic input energy, which are normally necessary for such mechanisms.

The fact that Pd cathode shows compositional changes after electrolysis in heavy water, prompted us to revisit the mechanism. Earlier, enrichment of Rhenium and Silver was observed on used palladium cathode after electrolysis in D_2O[4]. Subsequently, evidence of Gold and Silver was reported in another study[5]. These all indicated the possibility of transmutation of the cathode material. In a seminal report by Enyo et al., transmutation in a Pd/H_2O electrolysis was found to be more concentrated along the scraped edge of the electrode, and was inferred that roughed surface, where the lattice defects are highly distributed, plays an important role for the nuclear reactions leading to transmutation via a series of nuclear reactions involving highly energetic H atoms approaching Pd[6]. In fact, it is well known that, Pd-metal, when bombarded with highly energetic proton, deuteron or α-particles

[1]Bio-Organic Division, Bhabha Atomic Research Centre, Trombay, Mumbai 400085, India. [2]Chemistry Division, Bhabha Atomic Research Centre, Trombay, Mumbai 400085, India. [3]Department of Space, Planetary & Astronomical Sciences & Engineering, Indian Institute of Technology, Kanpur 208 016, India. [4]Department of Physics, Indian Institute of Technology, Kanpur 208 016, India. [5]Solid-State Physics Division, Bhabha Atomic Research Centre, Trombay, Mumbai 400085, India. [6]Radiochemistry Division, Bhabha Atomic Research Centre, Trombay, Mumbai 400085, India. [7]Electronics Division, Bhabha Atomic Research Centre, Trombay, Mumbai 400085, India. [8]Radiological Physics & Advisory Division, Bhabha Atomic Research Centre, Trombay, Mumbai 400085, India. [9]Molecular Biology Division, Bhabha Atomic Research Centre, Trombay, Mumbai 400085, India. [10]Homi Bhabha National Institute, Anushaktinagar, Mumbai 400094, India. ✉email: tgadly@barc.gov.in; dibakarg@barc.gov.in

generated from particle accelerators, results into transmutation of Pd to new elements along with generation of neutrons. For example, ^{105}Ag ($T_{1/2} = 41.29$ d) could be produced via ^{105}Pd (p, n) and ^{104}Pd (d, n) reactions, and, similarly, ^{106}Ag ($T_{1/2} = 8.28$ days) could be obtained via ^{106}Pd (p, n) and ^{106}Pd (d, 2n) reactions on the Pd target[7]. However, in electrolysis, the incident energy is relatively small and the standard fusion reactions are expected to have a very small rate. It has been argued that a different class of processes, which get leading contribution at second order in quantum perturbation theory, might have much higher rates and may be observable[8–11]. Herein, a highly reproducible, portable neutron generator has been designed and demonstrated using palladium metal cathode during electrolysis of heavy water. We envisaged that, in the experiment under consideration, many different reactions may contribute. Primarily, we postulated the presence of following exothermic reactions, such as, ^{106}Pd(d,n)^{107}Ag and ^{108}Pd(d,n)^{109}Ag, due to the presence of silver and neutrons in the final state, and we focused on these reactions for our theoretical calculations. Also, the basic idea on how the strong Coulomb repulsion is evaded in this case has been explained earlier[10,11] and reviewed later in this paper. This experimental evidence, alongwith strong theoretical explanation, may also lead to find newer materials for effective neutron generation.

Neutron generation

The prototype neutron generator (Prototype Reactor for Acquiring Neutron, PRAN), containing heavy water, was fabricated using Pd as cathode and Pt as anode as shown in Fig. 1, which represents a picture of PRAN equipped with a Digital Radiation Survey Meter (DSM).

The cathode and anode materials were fully characterized using Energy-dispersive X-ray spectroscopy (EDX) and Energy Dispersive X-ray Fluorescence spectroscopy (EDXRF). The composition of both are listed in Tables 1, 2 and Fig. 2. The same materials were used throughout the studies using PRAN.

Neutron generation from PRAN were initially detected using different detectors, viz. CR-39, epoxy resin and ^{3}He detectors. The CR-39 solid state nuclear track detector (SSTNDN) detect neutrons via its interaction with hydrogen in CR-39 polymer to produce recoil protons, which create damages in the detector sheet[12]. These damages were seen in our system when the unexposed CR-39 solid state detector (Fig. 3A) was placed inside the PRAN device at a distance of 2 cm from palladium metal electrode during the electrolysis with heavy water, after proper chemical etching (Fig. 3B,C). The image of CR-39 detector taken by the microscope confirmed the presence of neutron close to the point of generation in PRAN. These damages, after proper etching, could be counted in an optical system to evaluate neuron dose. CR-39 detector deployed inside and on the top of the glass beaker registered cumulative doses of 1.24 and 0.8 mSv respectively for a duration of 192 h. These results corroborated with the findings using epoxy resin, where direct visualization of neutron tracks could be obtained by microscopy without any prior chemical etching treatment (Fig. 3D,E). In our system, fast neutrons as well

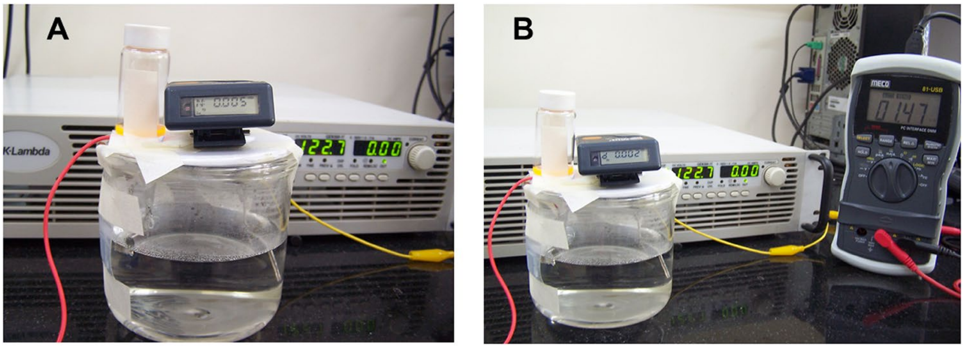

Fig. 1. Image of PRAN reactor showing (**A**) neutron dose during electrolysis using DSM monitor, (**B**) Gamma dose during electrolysis using DSM monitor.

Elements characterized by EDXRF	Cathode (Pd)	Anode (Pt)
Pd	99.1 ± 0.3	
Re	0.33 ± 0.03	
Ca	0.26 ± 0.07	1.7 ± 0.3
Pt	0.20 ± 0.04	98.2 ± 0.3
Fe	0.19 ± 0.05	0.12 ± 0.01
Hg	0.08 ± 0.01	
Cu	0.010 ± 0.001	
Ni	0.007 ± 0.002	

Table 1. Characterization data for cathode (Pd) and anode (Pt) material before electrolysis, obtained using EDXRF.

Element	Line type	Apparent concentration	k ratio	Wt%	Wt% sigma	Standard label
O	K series	2.38	0.00800	9.83	1.90	SiO2
Na	K series	0.89	0.00376	2.08	0.60	Albite
Pd	L series	55.03	0.55028	88.09	1.94	Pd
Total:				100.00		

Table 2. Weight percentage of elements present in palladium electrode before electrolysis obtained using EDAX.

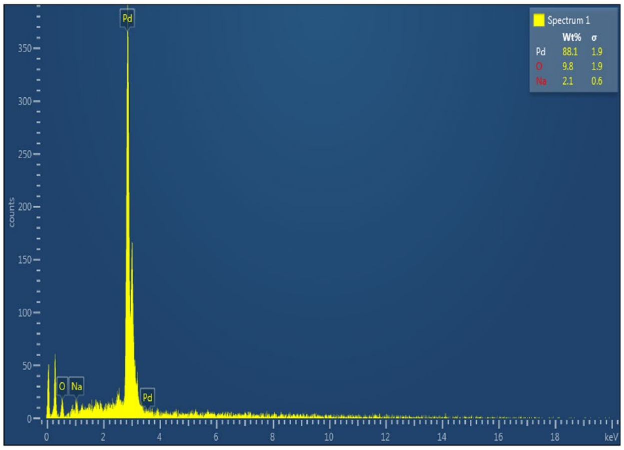

Fig. 2. EDX analysis of palladium metal electrode before electrolysis.

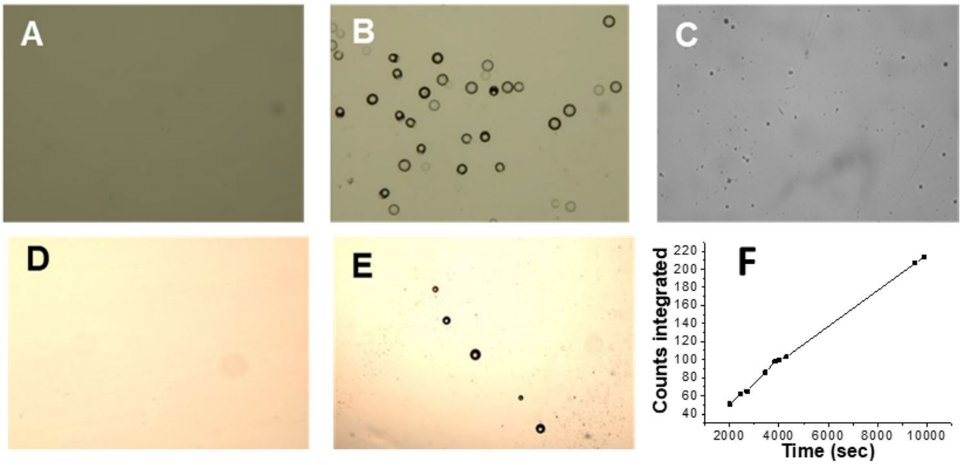

Fig. 3. (**A**) Blank image of CR-39 under × 10 magnification. (**B**) Irradiated CR-39 with PRAN reactor, image under × 40 magnification, obtained after chemical etching. (**C**) Irradiated CR-39 with PRAN reactor, image under × 10 magnification, obtained after chemical etching. (**D**) Blank image of epoxy resin under × 10 magnification. (**E**) Irradiated epoxy resin with PRAN reactor image under × 10 magnification. (**F**) Neutron counts from PRAN using ^{3}He detector.

as thermal neutrons were detected. In addition, the plot of neutron count vs time, obtained using gas filled ^{3}He detectors[13], was found to be linear (Fig. 3F), indicating thermal neutrons emission increased as a function of time after thermalization through high density polythene sheets.

Neutron generation by PRAN device was further validated by neutron counts shown by diamond radiation (Fig. 4). The pulse signals from the detector, recorded on a cathode ray oscilloscope (CRO), revealed pulses with varying heights, typically around 0.35 V as illustrated in Fig. 4A. The pulse height spectrum (PHS) has been shown in Fig. 4B. The lower threshold of the multi-channel analyzer (MCA) was set at approximately channel number 50, which was above the noise level. The PHS exhibited pulse heights ranging from channel number 600 to channel number Z, which corresponded to the elastic and inelastic scattering of neutrons within the diamond

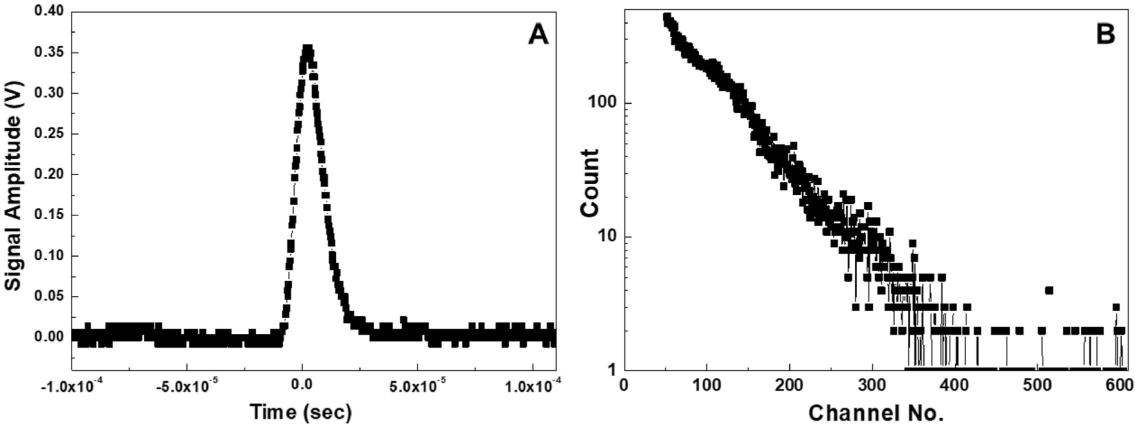

Fig. 4. (**A**) Pulse signal recorded on cathode ray oscilloscope; (**B**) PHS of neutrons obtained by multi-channel analyzer.

material. Therefore, the diamond radiation detector substantially indicated that the signal detected was that of neutron generated from the PRAN electrodes with an energy of 350 keV.

Theoretical explanation

As mentioned in the introduction, there may be many different processes which may contribute in this experiment. Here, we focused on two such processes, which convert palladium to silver with the production of neutrons, and can support the experimental evidence of the presence of silver and neutrons in the final state. We followed the formalism developed earlier[8–11] and assumed that these are assisted by another particle Y in the medium[8–11]. The particle Y could be an impurity ion in the medium or another palladium ion. Specifically we considered the following reactions.

$$_{46}{}^{106}Pd + d + Y(k_{Yi}) \rightarrow {}_{47}{}^{107}Ag + n + Y\left(k_{Yf}\right), \tag{1}$$

and

$$_{46}{}^{108}Pd + d + Y(k_{Yi}) \rightarrow {}_{47}{}^{109}Ag + n + Y\left(k_{Yf}\right), \tag{2}$$

which have Q values of 3.56 and 4.26 MeV, respectively. Other reactions, similar to these, are also possible which may produce an unstable isotope of Silver. Due to Coulomb repulsion, these processes were expected to be very strongly suppressed. However, herein, we considered a reaction which starts at second order in perturbation theory, with the transition amplitude from initial $|i\rangle$ to final state $|f\rangle$, given by[14],

$$\langle f|T(t_0,t)|i\rangle = \left(-\frac{i}{\hbar}\right)^2 \sum_{n=1}^{\infty} \int_{t_0}^{t} dt' e^{i(E_f - E_n)t'/\hbar} \langle f|H_I(t')|n\rangle \int_{t_0}^{t'} dt'' e^{i(E_n - E_i)t''/\hbar} \langle n|H_I(t'')|i\rangle,$$

where the sum over n goes from 1 to ∞, i.e. over all eigenstates of the unperturbed Hamiltonian. The process involved two interactions, the first involving transition from initial state to an intermediate state $|n\rangle$, while the second taking the intermediate state to final state. Furthermore, we needed to sum over eigenstates of all energies in the intermediate state as indicated by the sum over n in the above equation. Due to the presence of arbitrarily high energy states, the Coulomb barrier might be evaded. It is important to point out that energy is not conserved at each vertex although there is overall energy conservation[15]. At the first vertex we essentially formed a short-lived wave packet which did not have well defined energy. Hence it was not meaningful to impose energy conservation at this vertex. Despite the presence of such states of arbitrarily high energy, it was found that the overall rate of such reactions was negligible if the intermediate states were the standard free space wave functions[9–11]. This happened since we obtained contributions from a range of intermediate state energy eigenvalues and they all summed up destructively. Remarkably, the rate was sizeable if the wave functions were localized, as expected inside a medium in the presence of disorder, analogous to the well known phenomenon of Anderson localization[16]. This was explicitly shown earlier[10], where the authors performed a direct quantum mechanical calculation using a spherically symmetric potential model. The rate was found to be fairly large provided the potential is such that the eigenstates are localized. This calculation can be directly applied to fusion of light nuclei but may not be applicable for intermediate states of very high energy required for fusion of a light nucleus with a heavy nucleus. In the present case, dominant contribution was obtained from intermediate states of rather large energy eigenvalues and hence these states had large wave number $k = |\overrightarrow{k}|$. For such large k values we did not expect localization. However, as discussed earlier[11], and explained below, we only needed localization in the direction transverse to the large wave vector. This could be accomplished in a medium in the presence of disorder. The phenomenon of localization worked due to the medium potential experienced by the nuclear particles, such as deuteron. Hence, in our case, deuteron experienced a repulsive potential due to all medium ions. The deuteron wave function decayed at all such sites. It is well known that if the medium ions form a disordered system, rather than a periodic lattice, then all states below a certain energy are localized[15]. Herein, we were interested in states which have high energy and very large component of the wave vector in one direction, taken to be the z-axis. However the components of wave vector in the transverse direction were small. Hence it was reasonable to assume that the wave function will be delocalized in the z direction and localized in the transverse direction. We assumed that the scale of localization is the typical medium scale of order 5–10 atomic units. This turned out to be sufficient to lead to nuclear fusion at observable rates.

The theoretical analysis of the process is similar to the calculation performed earlier[11]. We assumed that, in the initial state, deuteron formed a bound state with palladium. The wave function of this bound state was taken to be spherically symmetric with radius of the order of typical molecular length scale[11]. At the first interaction, the deuteron ion experienced the Coulomb potential of the particle Y, leading to momentum k_{Yf} of this particle. Its momentum in the initial state k_{Yi} was assumed to be negligible. The intermediate state consisted of a deuteron nucleus of a relatively high momentum. At the second vertex the deuteron nucleus underwent a nuclear reaction with palladium to produce silver and a free neutron. The reaction rate for the process at second order in perturbation theory was found to be,

$$\frac{dP}{dt} = \frac{8\hbar Z_Y^2\alpha^2c^2}{V\pi^2}\int_{-\infty}^{\infty} d^3k_2 \int_{0}^{\infty} \frac{dk_{Yf}}{k_{Yf}^2}\,\delta\left(E_{Ag}+E_2+E_{Yf}-Q\right)\left|\int_{-\infty}^{\infty}\frac{Ldk_z}{2\pi}\sum_{\substack{k_\rho\, =\, all\\ allowed\\ states}}\frac{M_{fn}M_{ni}}{E_n-E_i+E_{Yf}}\right|^2,$$

where E_{Ag}, E_2 and E_{Yf} are the kinetic energies of the final state particles, silver, neutron and the Y particle respectively, $\vec{k}_2$ is the neutron wave vector, $\vec{k}$ is the intermediate state deuteron wave vector and Q refers to the Q-value of the process. In the above equation the limits of the integrals over $\vec{k}_2$ (all components) and k_z are from $-\infty$ to $+\infty$, and that over k_{Yf} are from 0 to ∞. The sum over k_ρ is over all the allowed states[11]. Here we neglected the intial state kinetic energies. In the sum over intermediate states, we got dominant contribution from deuteron wave vector $\vec{k} \approx -\vec{k}_{Yf}$. We chose the coordinate system such that $\vec{k}_{Yf}$ points along the z-axis. In that case, $\vec{k}$ pointed dominantly along the negative z-axis. We splitted this vector into its z component k_z and the transverse component k_ρ. The dominant contribution was obtained from relatively small values of k_ρ. Hence, we assumed that, in the transverse direction, the wave function is confined in the medium, leading to discretized values of k_ρ. However, the component k_z took very large, negative, values. Hence we assumed that k_z took a continuous range of values and wave function, and is not localized along the z-axis. Therefore, the factor of 1/V in the above formula should be replaced by the number density of the Y particles in the experiment[8,11]. The details of the calculation of the matrix element M_{ni} as well as the sum over k_ρ and the integral over k_z are similar to that reported by us earlier[11].

The matrix element M_{fn} involved a nuclear transition and had dimensions of $(\text{length})^{3/2} \times$ energy. The length factor arose since we have extracted an overall factor of $1/V^{3/2}$, which corresponded to the neutron wave function normalization, out of this matrix element. We proposed the following model for M_{fn},

$$M_{fn} \approx f_n e^{-b/\sqrt{E_d}},$$

where $b = 0.5 \times 31.28\ Z_d\ Z_{Pd}\ A^{1/3}\ \text{kev}^{1/2}$, $A = A_d\ A_{Pb}/(A_d + A_{Pb})$ and f_n is a factor with dimensions of $(\text{length})^{3/2} \times$ energy. Here Z and A refered to the atomic numbers and atomic mass numbers respectively of different nuclei. The exponential factor[17] is the standard formula for tunneling amplitude corresponding to energy E_d of the intermediate state deuteron. The factor f_n models the interaction strength for this strong interaction process. We assumed that it was approximately independent of energy and got an estimate on its value using typical values of the S_E factors for such processes[17]. These factors typically have values larger than 100 kev barns for such strong interaction processes. This value was consistent with the experimentally measured cross section[18] for deuteron induced reactions on palladium at high energies of order 24 MeV. Analogously, here we assumed a conservative value of 3000 keV $\text{fm}^{3/2}$ for this factor. This was based on the idea that the distance scale in this factor is the typical nuclear length scale. Inserting this in S_E we got an estimate of the energy scale. These factors could now be used to estimate f_n. This factor was best extracted experimentally and our assumed value may be off by an order of magnitude. However, this is sufficiently reliable for a preliminary estimate of the process.

For the assumed value of f_n the reaction rate turned out to be about 1 per second assuming presence of one d-Pd pair in the initial state. This was sufficiently large to be observable. We assumed that once the electrolysis process gets started, d ions start diffusing into the palladium lattice and form bound states with palladium. The actual rate depends on the number of such d-Pd bound states that get formed. In order to get some idea about the process, it was useful to consider the event count rate as a function of neutron energy. As shown in Fig. 5, it could be seen that the count rate decayed sharply to zero once the energy exceeded ~ 3 MeV. This was nicely consistent with the Q values of the processes which range from 2 to 4 MeV. The theoretically calculated neutron spectrum for the production of ^{107}Ag showed a monotonic decrease with energy starting from 1 MeV and also

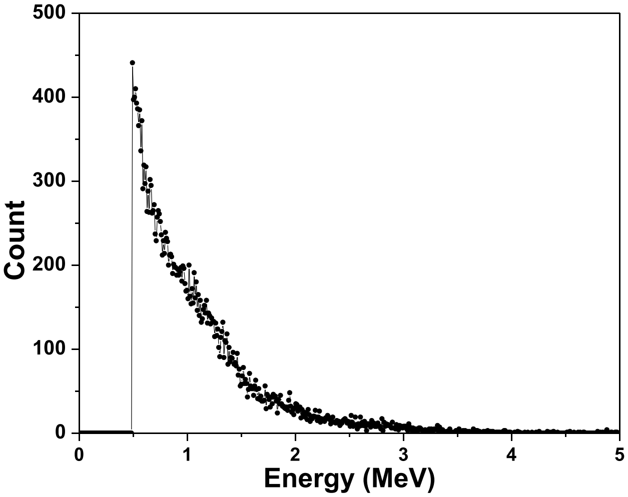

Fig. 5. Neutron spectrum from PRAN device showing count vs energy profile obtained by fast neutron diamond detector acquired for 3 h.

a decay a smaller energies. Hence, it captured the main features of the process under consideration. However, we understand that, a more detailed comparison is required to compute the rates of all the processes under consideration, taking into account a possible energy dependence of f_n.

Furthermore, to elucidate that nature of chemical species comprising the bound states of d-Pd resulting in the neutron generation from PRAN, splitting of D_2O was considered according to the following reaction (3).

$$D_2O \rightarrow D^+ + DO^-. \tag{3}$$

Ideally, following the electrolytic generation, the ions should recombine at electrodes forming D_2 and O_2 gases, at the cathode and the anode, respectively. However, absence of any discharge of D_2 gas from the cathode prompted us to revisit the reactions at the electrodes. Also, earlier models where the neutron generation have been explained by (d, d) fusion reactions, may not applicable in our experiments due to lack of observable excess heat generation and tritium production[19]. Hence, the experimental evidences indicated that the observed half-cell reaction during electrolysis of PRAN reactor is different from the known discharge of D^+ ions at the cathode. To explore the bound states of d-Pd as per the second order perturbation theory, three different clusters viz. (A) $Pd_{18}OD^-$, (B) $Pd_{18}OD^-$ with D^+ ion placed inside the Pd cluster, and (C) $Pd_{18}OD^-$ with D^+ ion placed outside the Pd cluster, were considered for theoretical simulations. The most stable structures for the systems, (A) $Pd_{18}OD^-$, (B) $Pd_{18}D_2O$, and (C), $Pd_{18}OD^-D^+$ are shown in Fig. 6. The relative stability of B and C were 338.4 kcal/mol and 358.7 kcal/mol, respectively, with respect to A. It was interesting to note that OD^- and D^+ combined to form D_2O if D^+ ions were placed inside the Pd cluster (Fig. 6B). However, it is also possible for deuterium atom to be embedded in the defects of palladium metal leading to the formation of Pd^{x+} metal ion as depicted in Eq. (4)[20].

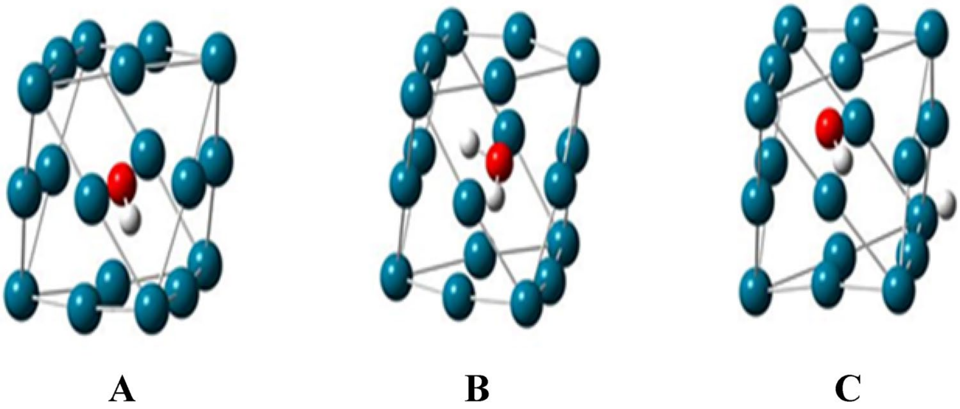

Fig. 6. Most stable structures of (**A**) $Pd_{18}OD^-$, (**B**) $Pd_{18}D_2O$ and (**C**) $Pd_{18}OD^-D^+$ at B3LYP level of theory. In each system, oxygen and deuterium atoms are shown by red and white color spheres and largest spheres are the Pd atoms. The images are made by using Jmol 14.3.15 (jmol.sourceforge.net).

As predicted, Pd^{x+} metal ion, formed from this plausible reaction, may act as one of the reactants i.e. Y, in the transmutation process Eqs. (1) and (2).

$$\mathrm{Pd} + \mathrm{xD}^{+} + \mathrm{xe}^{-} \rightarrow \mathrm{PdD_x}. \tag{4}$$

In addition, in cases where less energized D^+ ions were trapped in the Pd surface (Fig. 6C), D^+ ion interacted with the surface Pd atoms and got partially neutralized by charge transfer from the adjacent Pd atoms. Thus leading to the formation of d-Pd bounded state in accordance with the second order perturbation theory. As a result, nuclear reaction Pd(d,n)Ag has high probability as evident from the aforementioned proposed theory.

To verify the proposed Pd(d,n)Ag nuclear reaction experimentally, it was required to find transmutation signatures at the palladium electrode and if possible in the electrolyte too. Although the X-ray Diffraction pattern (Fig. 7) of the electrode after electrolysis did not infer much changes, SEM–EDX (Figs. 8, 9A) and a modified EDXRF method (Fig. 9B) was utilized to detect the formation of transmuted elements.

The composition of the electrode after electrolysis, as obtained from SEM–EDX analysis, have been listed in Table 3. EDXRF experiment with palladium electrode after electrolysis (Fig. 9B) confirmed presence of silver metal, which was not present in the palladium electrode before the start of the electrolysis experiment. The elemental mapping (EDS) (Fig. 10) also confirmed the presence of Ag in the electrode after electrolysis.

Spectro-electrochemistry, a coupled method of electrochemical and spectroscopy, was utilized to detect the intermediate or product species in the electrolyte formed during constant electrolysis. The absorption spectra obtained before and after electrolysis at different time intervals are shown in Fig. 11. Silver nanoparticles are known to exhibit a UV–Vis absorption maximum in the range of 400–500 nm with a characteristic double hump between 450 and 500 nm along with 900 nm because of surface plasmon resonance modes[21]. Before electrolysis, no absorption peak was found in the electrolyte in the wavelength region 300–1000 nm. However, after 1 h of electrolysis, prominent peaks viz. at 488 nm, 502 nm, 613 nm and 910 nm was observed. The intensity of these absorption peaks increased with increasing time of electrolysis (1–6 h), which suggested the continuous

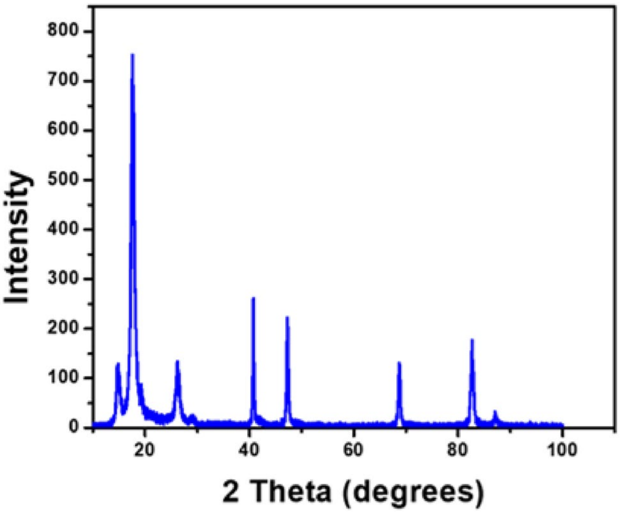

Fig. 7. X-ray diffraction pattern of Palladium metal electrode after electrolysis.

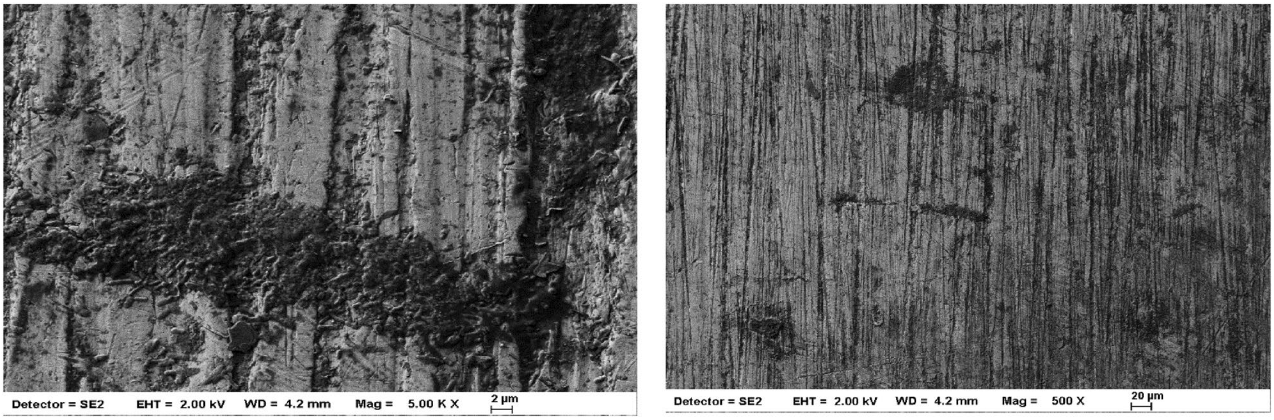

Fig. 8. SEM of Palladium metal electrode at (**A**) 2 µm scale, and (**B**) 20 µm scale after electrolysis.

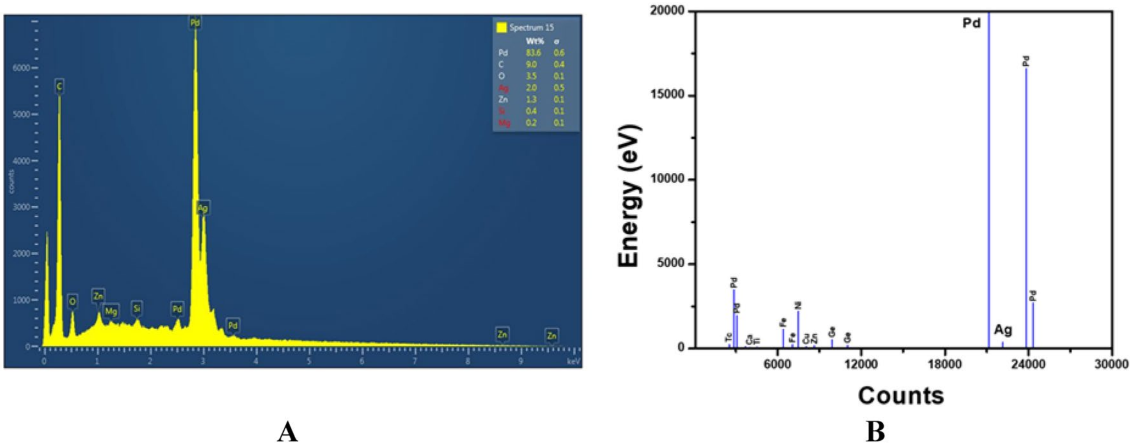

Fig. 9. (**A**) EDX of palladium metal electrode after electrolysis. (**B**) EDXRF of palladium metal after electrolysis indicating formation of silver.

Element	Line type	Apparent concentration	k ratio	Wt%	Wt% sigma	Standard label
C	K series	0.93	0.00925	9.02	0.43	C Vit
O	K series	0.33	0.00112	3.54	0.15	SiO_2
Mg	K series	0.03	0.00017	0.21	0.05	MgO
Si	K series	0.05	0.00043	0.41	0.05	SiO_2
Zn	L series	0.08	0.00077	1.28	0.12	Zn
Pd	L series	8.09	0.08091	83.59	0.63	Pd
Ag	L series	0.19	0.00191	1.95	0.52	Ag
Total				100.00		

Table 3. Weight percentage of elements present in Palladium electrode after electrolysis, as measured by EDX analysis.

transmutation of Pd cathode during electrolysis. These absorption peaks at 488, 502 and 910 nm were assigned for triangular silver (Ag) nano-particles[22]. Present studies reveal that, during electrolysis, Pd cathode showed compositional changes with generation of Ag nanoparticle in D_2O medium (Fig. 11)[23]. Formation of silver is a direct proof of Pd(d,n)Ag nuclear reaction of palladium metal with highly energetic deuterons, and thus supports the proposed theoretical model based on second order quantum perturbation theory.

Conclusion

Fast neutrons were produced from PRAN reactor which was detected by CR-39, epoxy resin, ^{3}He gas-filled detector and diamond radiation detector. The proposed theoretical model, based on second order perturbation theory, predicted transmutation of Pd cathode which was experimentally verified by EDX and EDXRF techniques. The reproducibility of the electrochemical cell in generating neutrons was also checked in multiple runs spanning for 7 days in each cycle. This is one of the rare examples of a neutron generating electrolytic cell, wherein the processes have been experimentally and theoretically validated. We hope that this would lead to a new paradigm in explaining the hidden nuclear reactions in similar systems.

Methods

Cathode material, anode material and Araldite (Pidilite Industries epoxy resin) was purchased from local vendor in Mumbai, India. Virgin D_2O (> 99.9%) was supplied by ROD, BARC, Mumbai. CR-39 detectors were supplied by RP&AD, BARC, Mumbai. Constant voltage power supply and nuclear electronics were provided by SSPD, BARC, Mumbai. Indigenously built ^{3}He detectors and diamond detectors were provided by SSPD and Electronics Division, BARC, Mumbai. Scanning Electron Microscopy (SEM) was performed using SEM-Carl Zeiss, UK coupled with Energy Dispersive X-ray spectroscopy (EDX)-INCA Energy 250, Oxford Instruments. For SEM, Sample was prepared on a clean glass slide and sputtered with gold using standard methods. The scanning of images was performed at an accelerating voltage of 10 keV and EDX spectra were obtained between 0 and 20 keV. X-ray Diffraction (XRD) analysis was done in Rigaku Smart Lab (9W) Wide angle XRD instrument. The experiment was performed with a scan from 5° to 80° with 3 degrees per minute at 6 W power. Spectro-electrochemical experiments were carried out by coupling the voltage supplier with an optics spectrophotometer (Ocean) with a QE 65000 detector fitted with a dip-probe assembly in which the spectrochemical dip probe was placed inside a glass cell containing the test solution of D_2O. A Pd plate (30 mm × 30 mm) was placed close to the dip probe

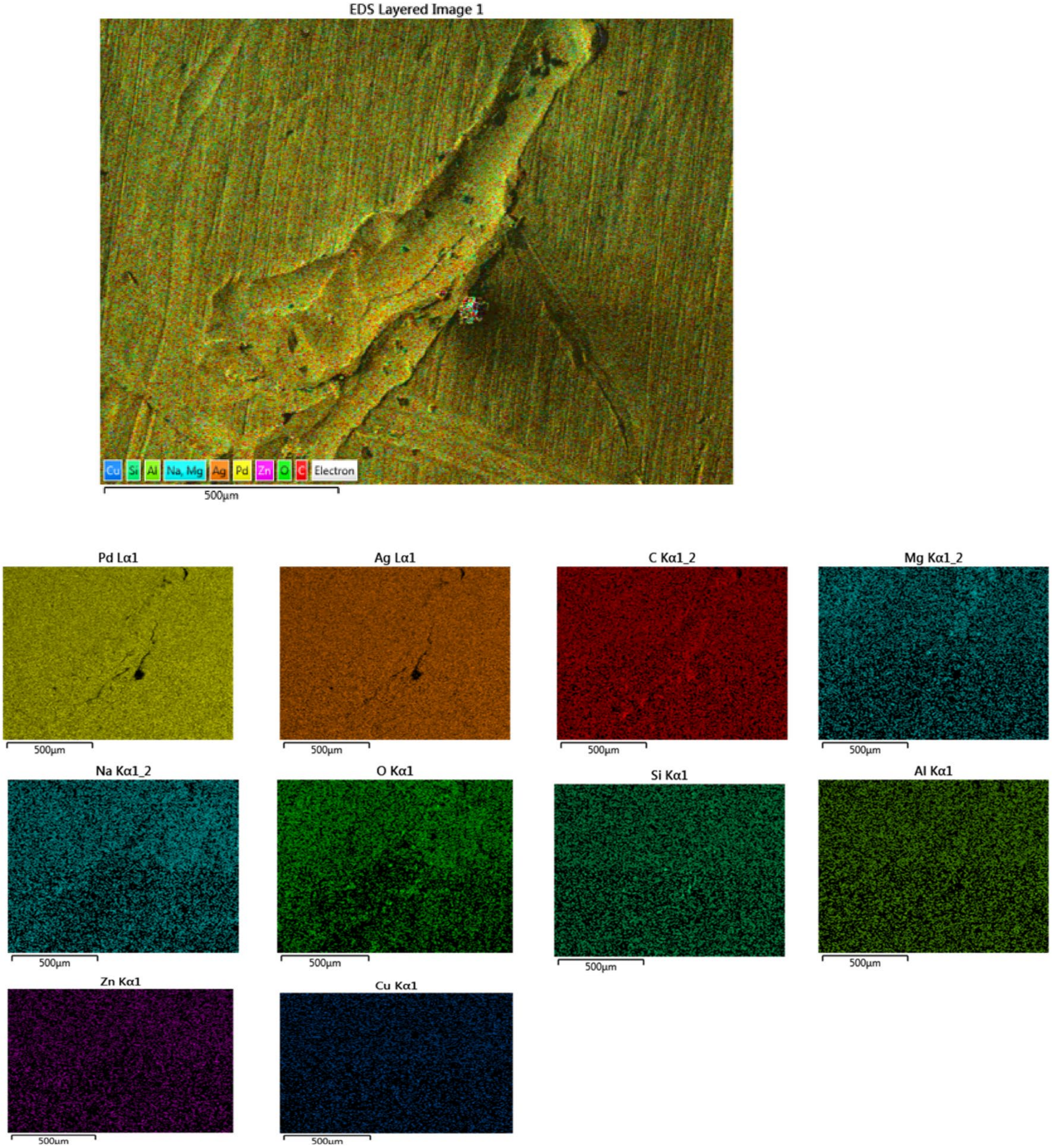

Fig. 10. EDX layered image and elemental mapping of palladium metal electrode after electrolysis.

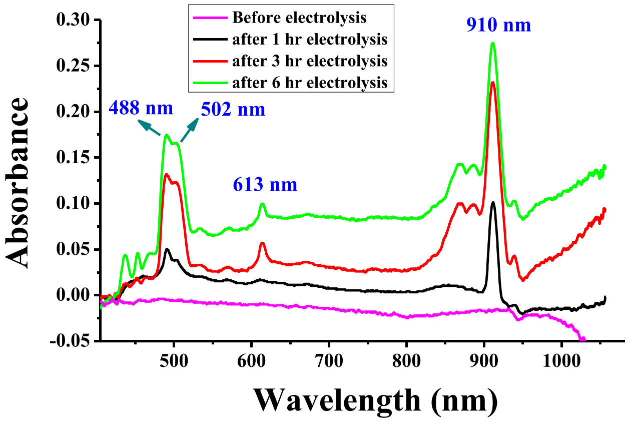

Fig. 11. Changes in absorption spectra of D_2O with increasing time of electrolysis.

and used as the working electrode with Ag/AgCl as the reference electrode and Pt rod as counter electrode. The absorption spectra were recorded in presence of applied potential at various times in in-situ mode.

A prototype neutron generator (Prototype Reactor for Acquiring Neutron, PRAN) was devised with cylindrical glass container (Diameter = 70 mm, Height = 150 mm) containing 300 mL virgin heavy water using Palladium (Pd) metal electrode having square geometry (30 mm × 30 mm × 0.5 mm) and thin cylindrical platinum (Pt) electrodes (length = 50 mm and diameter = 2.0 mm). A constant DC voltage supply at 122.7 V was applied, with Pd electrode as cathode and Pt electrode as anode. During initial experiments, electrolysis was carried out for a period of 3 h, and later for a period of 4 days (96 h). Generation of neutrons was assessed using solid state CR-39 detectors, diamond detectors as well as gas filled ^{3}He detector. Diamond radiation detector was kept on the top surface of PRAN device. A test-tube containing transparent and viscous epoxy resin was immersed inside the heavy water close to Pd electrode. Background radiation was corrected using blank CR-39, epoxy-resin and ^{3}He detectors. DC potential was varied from 30 to 122.7 V for optimization. Corroboration of validity of neutron generation was also checked with 5 MeV plutonium-beryllium (Pu/Be) source with novel epoxy resin, CR-39, diamond radiation detector and gas filled ^{3}He detectors.

Neutron detection by solid state CR-39 detector[24]

CR-39 detectors (procured from M/s TASL, UK) of size 1 cm × 1 cm × 0.75 mm loaded and double sealed in polyethylene pouch were mounted on the top (2 cm from electrode), inside beaker dipped in electrolyte 1 cm from the electrode of the PRAN device. After irradiation, CR-39 detectors were processed using chemical etching in 7 N potassium hydroxide (KOH) solution for 7 h. Subsequently detectors were washed under flowing water and dried overnight. The number of tracks per unit area in blank CR-39 detector were measured and then the same measurement was done in the etched sample. Subsequently, tracks were counted under an optical microscope (Axiostar Plus, Carl Zeiss India Pvt. Ltd.) which has a motorized stage (Prior Scientific, UK), frame grabber card (IDS FALCON) and a CCD camera (WATEC 902B) along with an Image analysis software (IMAGE PRO plus) is used for counting tracks under either × 40 or × 10 magnification. The imaging system is calibrated for track counting by irradiating CR-39 detectors to ^{241}Am-Be neutron source (yield 2.5×10^6 n/s) at distance of 50 cm in air and calibration factor was found to be 1.2×10^{-3} mSv tracks^{-1} cm^{-2}. Shape based filtering algorithm in the imaging system which uses diameter and roundness factor of tracks to identify genuine particle tracks, was used in the measurement.

Neutron detection by novel epoxy resin detector

Transparent, semi-liquid epoxy resin detector was used for this purpose. A 5 mL glass test tube containing epoxy resin was kept at a distance of 2 cm from Palladium metal electrode which acted as a cathode during electrolysis with heavy water. Identical resin was used to calibrate the detection of fast neutrons with a 5 MeV Pu/Be source.

Neutron detection by gas filled ^{3}HE detector

Gas filled ^{3}He detectors were used by placing a meter-long detector close to the PRAN vessel. High density polythene (HDP) plastic sheets of thickness 1 cm was kept between the PRAN device and ^{3}He detector. The neutron counts were measured after background correction.

Neutron detection by diamond radiation detector

Neutron generation by PRAN device was further validated by neutron counts shown by diamond radiation Neutrons interact with diamond through various mechanisms depending on their energy. Typically, neutrons undergo elastic and inelastic scattering with carbon nuclei, transferring a fraction of their energy to the carbon atoms. For instance, fast neutrons with an energy of 14.2 MeV from Deuterium–Tritium (D–T) reaction undergo multiple nuclear reactions with carbon, leading to the production of charged particles that deposit their energy in the detector[25]. The energy deposition in the detector generates charge carriers, which produce a fundamental electrical signal upon collection through the application of an electric field.

The diamond detector and the back-end electronics set up has been depicted in Fig. 12. The back-end electronics setup comprised a charge-sensitive preamplifier (CSP), a shaping amplifier (SA), and a multichannel analyzer (MCA), as depicted in Fig. 12. The CSP and SA integrated the charge carriers and generated electric

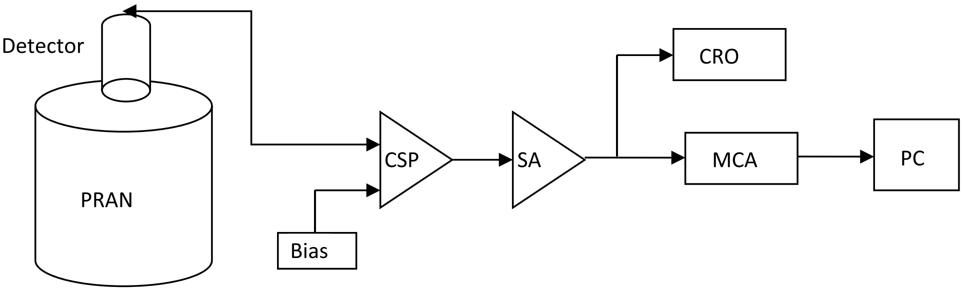

Fig. 12. Schematic of neutron detection using diamond detector with back-end electronics.

pulses, which were monitored on a cathode-ray oscilloscope (CRO) and digitized using the MCA to record the pulse height spectrum on a personal computer (PC).

The pulse signals from the detector were recorded on a CRO. The pulse height spectrum (PHS) was obtained using the multichannel analyzer (MCA) and recorded on a PC. The lower threshold of the MCA was set at approximately channel number 50, which was above the noise level.

Theoretical calculations

Different feasible nuclear processes were analysed using the second order time dependent perturbation theory. B3LYP hybrid density functional was used to carry out geometry optimizations. The B3LYP density functional consisted of Becke's three parameter non-local exchange (B3) and the Lee–Yang–Parr (LYP) nonlocal correlation (B3LYP). Quasi Newton–Raphson based algorithm was used for geometry search of various clusters. Gaussian type triple split valence basis functions, viz. 6–311 ++ G** were used for O and H atoms and double split valence, namely, 3–21G* basis sets for Pd atom were used in the calculations. GAMESS suites of ab initio program systems on a LINUX cluster platform was employed to carry out all electronic structure calculations[26]. Molecular geometries and orbitals were visualized by using the MOLDEN and MOLEKEL program systems[27,28]. Initially, a Pd cluster consisting of 19 atoms was considered as base model to make various clusters consisting of OD^- and D^+ ions.

Modified EDXRF analysis

All EDXRF measurements were carried out using EX 3600M, Xenemetrix, Israel, having a Rh-anode X-ray tube, silicon drift detector and in-built software, nEXt, for spectral analysis. The optimized acquisition parameters for the present measurements were: X-ray tube potential: 35 kV, emission current: 100 µA, time: 300 s, medium: air, throughput: high, range: 40 keV. In all these procedures, Ag in the sample were calculated using the intensities of interference-free characteristic X-rays. In general, X-ray tubes employed in EDXRF systems are of low power (~ 10 W when used as primary excitation source and ~ 100 W in the secondary excitation geometry) and, therefore the associated high voltage supplies are very economic, compact and portable. The broad band of X-ray energies emerging from the X-ray tube when used directly has the advantage of exciting a wide range of elements with nearly same efficiency, though unfortunately, it also produces a high spectral background due to scattering of incident radiation by the sample. In the modified method, the low power X-ray tubes with transmission targets of Molybdenum, Rhodium etc. was coupled with an additional filter placed between the tube and the sample. This moderated the primary broad band radiation to an approximately mono-energetic source. Eventually, the modified EDXRF analysis allowed qualitative as well as quantitative analysis of almost all the elements from beryllium to uranium irrespective of whether it is a low Z or high Z element present in the sample. This procedure was used throughout for the determination of Ag.

Data availability

All data generated or analysed during this study are included in this published article. More information about the datasets used and/or analysed during the current study are available from the corresponding author on reasonable request.

Received: 19 March 2024; Accepted: 19 August 2024

References

1. Niranjan, R., Srivastava, R., Joycee, J. & Joshi, K. D. Development of a portable pulsed fast ≥ 10^6 neutron generator based on a flexible miniature plasma focus tube. *Plasma Phys. Control. Fusion* **65**, 075010 (2023).
2. Fleischmann, M., Pons, S. & Hawkins, M. Electrochemically induced nuclear fusion of deuterium. *J. Electroanal. Chem.* **261**, 301 (1989).
3. Lohr, L. L. Electronic structure of palladium clusters: Implications for cold fusion. *J. Phys. Chem.* **93**, 4697–4698 (1989).
4. Rolison, D. R. & O'Grady, W. E. Observation of elemental anomalies at the surface of palladium after electrochemical loading of deuterium or hydrogen. *Anal. Chem.* **63**, 1697 (1991).
5. Dash, J., Noble, G. & Diman, D. Surface morphology and microcomposition of palladium cathodes after electrolysis in acified light and heavy water: Correlation with excess heat. *Trans. Fusion Technol.* **26**, 299–306 (1994).
6. Ohmori, T., Mizuno, T., Kurokawa, K. & Enyo, M. Nuclear transmutation reaction occurring during the light water electrolysis on Pd electrode. *Int. J. Soc. Mater. Eng. Resour.* **6**, 35–44 (1998).
7. Hermanne, A., Tarkanyi, F., Takacs, S. & Shubin, Y. N. Experimental determination of cross-section of alpha-induced reactions on ^{nat}Pd. *Nucl. Instrum. Methods Phys. Res. B* **229**, 321–332 (2005).
8. Kalman, P. & Keszthelyi, T. Forbidden nuclear reactions. *Phys. Rev. C* **99**, 054620 (2019).
9. Jain, P., Kumar, A., Pala, R. & Rajeev, K. P. Photon induced low energy nuclear reactions. *Pramana* **96**, 96 (2022).
10. Ramkumar, K., Kumar, H. & Jain, P. A toy model for low energy nuclear fusion. *Pramana* **97**, 109 (2023).
11. Jain, P. & Kumar, H. Medium assisted low energy nuclear fusion. http://arXiv.org/2403.04428.
12. Dhairyawan, M. P., Marathe, P. K. & Massand, O. P. Use of CR-39 solid state nuclear track detector in neutron personnel monitoring. *Radiat. Meas.* **36**, 435–438 (2003).
13. Piscitelli, F. *et al.* Verification of He-3 proportional counters' fast neutron sensitivity through a comparison with He-4 detectors. *Eur. Phys. J. Plus* **135**, 577 (2020).
14. Merzbacher, E. *Quantum Mechanics* (Wiley, 1998).
15. Halzen, F. & Martin, A. D. *Quarks and Leptons* (Wiley, 1984).
16. Lee, P. A. & Ramakrishnan, T. V. Disordered electronic systems. *Rev. Mod. Phys.* **57**, 287337 (1985).
17. Clayton, D. D. *Principles of Stellar Evolution and Nucleosynthesis* (The University of Chicago Press, 1968).
18. Ukon, N., Aikawa, M., Komori, Y. & Haba, H. Production cross sections of deuteron-induced reactions on natural palladium for Ag isotopes. *Nucl. Instrum. Methods Phys. Res. B* **426**, 13 (2018).

19. Mizuno, T. *et al.* Neutron evolution from a palladium electrode by alternate absorption treatment of deuterium and hydrogen. *Jpn. J. Appl. Phys.* **40**, L989–L991 (2001).
20. Guanqun, H., Guodong, L. & Yujie, S. Electrocatalytic hydrogenation using palladium membrane reactors. *JACS Au* **4**, 328–343 (2024).
21. Botasini, S., Dalchiele, E. A., Benech, J. C. & Mendez, E. Stabilization of triangular and heart-shaped plane silver nanoparticles using 2-thiobarbituric acid. *J. Nanopart. Res.* **13**, 2819–2828 (2011).
22. Harriet, K., Zhang, X. & Stulz, E. The temperature stability and development of a broadband silver nanofluid for solar thermal applications. *Energy Rep.* **7**, 87–96 (2021).
23. Ashraf, J. M., Ansari, M. A., Khan, H. M., Alzohairy, M. A. & Choi, I. Green synthesis of silver nanoparticles and characterization of their inhibitory effects on AGEs formation using biophysical techniques. *Sci. Rep.* **6**, 20414 (2016).
24. Pal, R., Biju, K., Thomas, R. G., Bakshi, A. K. & Sapra, B. K. Use of Zirconium capped CR-39 (Zr-CR-39) combination detector for high energy neutron dosimetry—Monte Carlo simulation studies and experimental validation. *Radiat. Meas.* **153**, 106747 (2022).
25. Kumar, A. & Topkar, A. A study of the fast neutron response of a single crystal diamond detector at high temperatures. *IEEE Trans. Nucl. Sci.* **65**, 630–635 (2018).
26. Schmidt, M. W. *et al.* General atomic and molecular electronic structure system. *J. Comput. Chem.* **14**, 1347–1363 (1993).
27. Schaftenaar, G. & Noordik, J. H. Molden: A pre- and post-processing program for molecular and electronic structures. *J. Comput. Aided Mol. Des.* **14**, 123–134 (2000).
28. Portmann, S. & Luthi, H. MOLEKEL: An interactive molecular graphics tool. *Chimia* **54**, 766–770 (2000).

Acknowledgements

The authors would like to express our heartfelt gratitude to Dr. A. K. Tyagi, BARC; Dr. Subir K. Ghosh, BARC; Dr. A. K. Satpati, BARC, Dr. P. A. Hassan, BARC, Dr. Mahesh Tiwari, BARC and Mr. Santosh Kumar, BARC for fruitful discussions.

Author contributions

T.G. conceived the project and designed experiments. S. P., S.G., S.K.P., S.D., A.K.P., A.S., A.K., R.P. & P.C. performed experiments. P.J. & H.K. performed theoretical calculations and edited the manuscript. T.G., A.K.P., C.A., A.K.B., S.V., B.S.P. & D.G. analysed and interpreted data. T.G. & D.G. wrote the manuscript with input from all authors.

Competing interests

The authors declare no competing interests.

Additional information

Correspondence and requests for materials should be addressed to T.G. or D.G.